Polymer 218 (2021) 123524

Contents lists available at ScienceDirect

Polymer

journal homepage: http://www.elsevier.com/locate/polymer

Magneto-responsive photochromic acrylic copolymer nanoparticles: An investigation into the mutual interactions and photoisomerization kinetics

Alireza Mouraki, Zeinab Alinejad, Samira Sanjabi, Hamid Salehi-Mobarakeh, Ali Reza Mahdavian *

Polymer Science Department, Iran Polymer & Petrochemical Institute, P.O. Box 14965/115, Tehran, 1497713115, Iran

ARTICLE INFO

Keywords:
Photochromic
Spiropyran
Magnetite
Miniemulsion polymerization
Stimuli-responsive

ABSTRACT

Photoresponsive and magneto-responsive smart materials have received specific attention. Here, novel bifunctional polyacrylic nanoparticles were prepared via miniemulsion polymerization in which, magnetite nanoparticles (10–15 nm) were resided in the core and poly (methyl methacrylate-co-spiropyran ethyl acrylate) (poly (MMA-co-SPEA)) was located in the shell. Chemical bonding of spiropyran onto the surface of magnetite provided their close vicinity, leading to effective interactions which have not been studied before. The interactions between the excited state of merocyanine (MC) zwitterion from spiropyran (SP) group and magnetic field of the superparamagnetic Fe_3O_4 NPs were investigated. The results revealed the existence of mutual interactions and successful increment in the absorption intensity (up to 176%) and optical stability, 9% changes in the rate of photoisomerization and increment in the half life time of MC isomers. These were achieved in the presence of magnetite as well as enhancement in the magnetic properties by 10% under UV irradiation at 365 nm. Such synergistic and two-way interactions between magnetic field of the superparamagnetic Fe_3O_4 NPs and the produced instant dipole moments in MC may offer a new route toward preparation of dual responsive nanocomposite particles for light-triggered magnetic switches, magnetic-triggered photo switches and simultaneous sensing and separation probes.

1. Introduction

Smart or stimuli-responsive polymers are high-performance polymers which have attained many attentions in recent years. Their properties can be changed based on external environmental stimuli such as temperature, humidity, pH, solvent, mechanical force, light, electrical or magnetic fields, ions, sound, enzymes and biomolecules [1–5]. The responses can be either physically or chemically like color or transparency, conductivity, permeability, solubility, shape and etc., but the changes must importantly be reversible [4,6]. Because of the non-destructive, harmless, quick and remote controllability of light, photoresponsive polymers are promising candidates in optics, photo-switches, photo-mechanical systems, micropatterning, and non-linear optical devices [7]. During photoisomerization of such compounds, some physicochemical properties including oxidation/reduction potential, refractive index, dielectric constant, geometrical structure and luminescence are changed in addition to their absorption spectra [8–10].

In the past 50 years, spiropyran as a photochromic compound has widely been studied according to its spectacular features. Upon UV irradiation, spiropyran (SP) to merocyanine (MC) isomerization occurs with an intense color change through ring opening and cleavage of C–O (spiro) bond to give zwitterion form. Merocyanine returns to the colorless closed SP by either visible light or heat [11,12]. Copolymerization has already been accepted as an efficient route for incorporation of spiropyran groups into a polymeric substrates [13–16]. As a result of chemical bonding between spiropyran and polymer chains, these photoresponsive copolymers represent prominent aspects including prevention of the dye leakage or aggregation, reducing the probability of undesired negative photochromism, enhancement in photostability and photofatigue resistance of the photoactive moieties [17,18].

Magnetic nanoparticles (MNPs) and magnetic composite nanoparticles are being applied in various fields such as magnetic resonance imaging (MRI), coatings, cell separation, catalysis, drug delivery systems, cancer therapy and magnetic separation due to their high response rate widely [19–22]. Among several MNPs, Fe_3O_4 NPs have been

* Corresponding author.
E-mail address: a.mahdavian@ippi.ac.ir (A.R. Mahdavian).

https://doi.org/10.1016/j.polymer.2021.123524
Received 8 September 2020; Received in revised form 7 December 2020; Accepted 7 February 2021
Available online 11 February 2021
0032-3861/

recognized as the best nominee because of their excellent features like reasonable biocompatibility, ease of synthesis and modification, high ability to control size and shape, proper chemical stability and remarkable magnetic properties [23,24]. These NPs, can be synthesized in both hydrophobic and hydrophilic media [25]. The synthetic methods include solvothermal [26], co-precipitation [27], polyol [28], sonochemical reactions [29], sol-gel [30] and thermal decomposition of the organometallics [24,31]. However, adjustment of the size (even below 20 nm) and morphology with narrow particle size distribution are still serious challenges to obtain superparamagnetic iron oxides nanoparticles (SPIONs) and can be achieved by thermal decomposition method preferably. Reaction time, heating rate, surrounding atmosphere, solvent, ligand and additives are the key points for this purpose [32]. On the other hand, several strategies are being employed for preparation of magnetic composite nanoparticles and encapsulation of MNPs in the polymer particles [33,34], particularly in emulsion-based systems [27]. Coverage of MNPs by polymeric shells will avoid their agglomeration, protect them against environmental effects, improve their chemical stability and reduce their toxicity [35].

Dual responsive polymeric nanoparticles to light and magnetic field are among the latest trends in smart materials. The exploitation of these polymeric nanoparticles in early diagnosis, MRI, targeted therapy, cell separation, drug delivery, sensors and nanodevices are developing now [36–39]. Osborne et al. [40] reported the synthesis of a reversible T_2 agent using magnetite NPs and spiropyran in MRI and evaluated the relaxation time in response to light irradiation. However, they did not study the relationship between photochromic and magnetic properties. In 2003, the intercalation of iron oxide NPs into photoresponsive amphiphilic spiropyran vesicles were investigated together with their interactions [41,42]. The observed aggregation after UV-irradiation led to an irreversible phenomenon as a drawback for responsive photochromic-magnetic systems. No close interaction between these two stimuli-responsive moieties was taken into consideration, i.e. through chemical bondings. Apart from this, prolonged UV irradiation (about 180 min) with minor enhancement in magnetic properties might be a questionable issue due to their poor mutual interactions.

To the best of our knowledge, there is not any specific study on the possible intervention between photoactive groups with magnetite nanoparticles after putting them together and in a close contact. In addition, such investigations may pave the way for preparation of light-triggered magnetic switches or memories, magnetic-triggered photoswitches and also simultaneous sensing and separation probes. In other words, the aim of this study is obtaining photoresponsive superparamagnetic nanoparticles with dual responsivity as well as studies on their mutual interactions. For real-time exploitations, desirable saturation magnetism with near zero loss of magnetization during magnetization-demagnetization cycles and optimized UV irradiation time for photo-magnetization should be considered essentially. This work reports the preparation of multifunctional composite nanoparticles with photochromic and magnetic properties. Spiropyran ethyl acrylate (SPEA) monomer and acrylic-modified Fe_3O_4 NPs were synthesized first. The polymer-magnetite nanoparticles (PMNPs) were then prepared by encapsulating Fe_3O_4 NPs with 10–15 nm size in poly (methyl methacrylate-co-SPEA) (poly (MMA-co-SPEA)) through miniemulsion polymerization. These new PMNPs with simultaneous response to UV–Vis light and magnetic field were in the range of 65–95 nm and the stimuli-responsive compartments were all covalently bonded in each nanoparticle. Next, photochromic behavior of PMNPs under UV–Vis irradiation, magnetic parameters, photofatigue resistance and long-term photostability were investigated comprehensively. Covalent bonding and embedment in the polymeric matrix provided the situation to study the probable and exclusive interactions. Herein, the correlation between the magnetic field of Fe_3O_4 NPs and the photochromic properties of spiropyran groups has been considered as a novel aspect.

2. Experimental section

2.1. Materials

2,3,3-Trimethylindolenin (Sigma-Aldrich Chemical Co.), iron (III) acetylacetonate ($Fe(acac)_3$) (Sigma-Aldrich Chemical Co.), 1,2-hexadecanediol (Sigma-Aldrich Chemical Co.), oleic acid (Sigma-Aldrich Chemical Co.), oleylamine (Sigma-Aldrich Chemical Co.), diphenyl ether (Merck Chemical Co.), 3-(trimethoxysilyl)propyl methacrylate (MPS) (Sigma-Aldrich Chemical Co.), sodium dodecyl sulfate (SDS) (Sigma-Aldrich Chemical Co.) as an anionic surfactant, and Triton X-100 (Merck Chemical Co.) as a nonionic surfactant were used without further purification. All solvents, 2-bromoethanol, 2-hydroxy-5-nitrobenzaldehyde, methyl methacrylate (MMA), triethylamine, acryloyl chloride (AC), sodium bicarbonate ($NaHCO_3$) as a buffer, hexadecane (HD) as a co-stabilizer and potassium persulfate (KPS) as the initiator were supplied by Merck Chemical Co, and used as received. Tetrahydrofuran (THF) was dried over sodium and distilled off. Other solvents and all reagents were used without purification. Deionized (DI) water was used in all experiments.

2.2. Synthesis of 1′-(2-acryloxyethyl)-3′,3′-dimethyl-6-nitrospiro-(2H-1-benzopyran-2,2′-indoline) (SPEA)

SPEA was synthesized in a four-step process and based on the previously reported procedure by our group [11]. Briefly, synthesis of SPEA involved following steps: (1) substitution nucleation reaction between 2,3,3-trimethylindolenine and 2-bromoethanol in methyl ethyl ketone (MEK) under N_2 to give 1-(2-hydroxyethyl)-2,3,3-trimethyl-3H-indolium bromide pink solid; (2) isomerization reaction of the product from step (1) in the presence of KOH/H_2O to yield (R/S)-9,9,9a-trimethyl-2,3,9,9a-tetrahydrooxazolo[3,2-a] indole (R/S) as a yellow oil; (3) condensation reaction between the product from step (2) and 2-hydroxy-5-nitrobenzaldehyde in ethanol (EtOH) under N_2 which gives (R/S)-2-(3′,3′-dimethyl-6-nitro-3′H-spiro-[chromene-2,2′-indole]-1′-yl) ethanol (R/S) (SPOH) as a purple solid; (4) modification of SPOH with acryloyl chloride in dry THF in the presence of triethylamine to produce yellow precipitate of SPEA.

2.3. Preparation of Fe_3O_4 NPs and the modified magnetite (m-Fe_3O_4) nanoparticles

Fe_3O_4 NPs were synthesized via a thermal decomposition method [24]. 2.12 g (6 mmol) $Fe(acac)_3$, 4.81 g (18 mmol) oleylamine, 5.08 g (18 mmol) oleic acid and 7.75 g (10 mmol) 1,2-hexadecanediol were dissolved in 60 mL diphenyl ether and the reaction mixture was heated to 200 °C and maintained at this temperature for 1 h under a flow of nitrogen gas, while stirring at 500 rpm. Then the mixture was further heated to the reflux conditions (~260 °C) and kept for 2 h, until a stable black suspension was obtained. The resulting black mixture was cooled down to room temperature. At ambient conditions, 25 mL ethanol was added and the synthesized Fe_3O_4 NPs were separated by a magnet, followed by three times washing with ethanol and drying for 48 h under vacuum at 40 °C.

Next, the prepared Fe_3O_4 NPs were modified by 3-(trimethoxysilyl) propyl methacrylate (MPS). 1 g of Fe_3O_4 NPs was dispersed in 70 mL toluene under ultrasonic irradiation for 10 min. The mixture was transferred to a three-necked round bottom flask equipped with mechanical stirrer, condenser and nitrogen gas inlet. 1 g MPS was added to the above dispersion and stirred at 700 rpm and 75 °C for 6 h. The product (m-Fe_3O_4 NPs) was washed with ethanol (3 × 25 mL), separated with a magnet and dried for 24 h under vacuum at 25 °C.

2.4. Preparation of m-Fe_3O_4@poly(MMA-co-SPEA) nanocomposite particles through miniemulsion polymerization

The oil phase containing MMA, hexadecane and m-Fe_3O_4 NPs was prepared and probe-sonicated for 2 min to achieve a good dispersion of m-Fe_3O_4 NPs in MMA. To proceed miniemulsion polymerization, the above dispersion was mixed with a SDS solution (as ionic surfactant), Triton X-100 (as non-ionic surfactant) and $NaHCO_3$ (as buffer) in DI water and then, SPEA was added to this mixture. The mixture was probe-sonicated for 20 min in an ice bath to form a pre-emulsion, followed by transferring into a three-necked round bottom flask equipped with a mechanical stirrer, condenser and nitrogen gas inlet. After addition of KPS as the initiator at 70 °C and stirring at 300 rpm, polymerization reaction was continued for 4 h to obtain stable latex with high conversion (>95%) with almost no coagulum. The starting materials and their amounts in preparation of typical latex (MNP0-S0) have been listed in Table 1.

Samples with various contents of SPEA and m-Fe_3O_4 NPs, and similar to the above recipe were prepared and amounts of stimuli-responsive components have given in Table 2.

Finally, the latexes were coagulated by ethanol (as the non-solvent) to determine the amount of covalently bonded SPEA to the acrylic backbone. This was estimated to above 97% based on absorbance of the remained serum relative to the standard solution. In addition, this copolymerization efficiency was also confirmed, while the nanoparticles were separated magnetically instead of coagulation and were analyzed by absorption intensity measurement.

2.5. Characterization

The products were identified by means of a FT-IR BRUKER-IFS48 spectrophotometer (Germany) with a resolution of 4 cm^{-1} in the range of 400–4000 cm^{-1}. A small amount of sample powder was grinded with KBr and the mixture was pressed into a disk for analysis. Photochromic properties of PMNPs were evaluated through UV–Vis analysis by a Shimadzu-UV2550 UV–Vis Spectrophotometer (Japan). For these analyses, the initial latexes were diluted to about 0.5 wt% with DI water. A UV lamp (365 nm), CAMAG 12VDC/VAC (50/60 Hz, 14VA, Switzerland) was used to stimulate the changes in structure and absorption bands of the photochromic SP moieties. Moreover, the source for visible light was a 15 W LED lamp with white light. In all investigations, UV and Vis irradiations time were set 5 min for all the samples. X-ray diffraction (XRD, D-5000 Diffractometer model, Siemens, Germany) measurements were carried out using a radiation source of Cu Kα (2θ: 10–90) with a step size of 0.02° and a scan step time of 1 s.

Particle size and polydispersity index (PDI) of the diluted latexes (up to 100 folds) were measured by dynamic light scattering (DLS), while zeta potential of the diluted photochromic-magnetic latexes was determined by micro-electrophoretic method, both using Malvern Zetasizer ZEN3600. Scanning electron microscopy (SEM, Vega II, TESCAN Instrument, Czech Republic) was employed to study size and morphology of the obtained PMNPs. One drop of the diluted latex was placed on a sample holder and dried under vacuum at 25 °C. The sample was then evacuated under vacuum and gold-sputtered by using EMITECH K450x sputter coater (England). EDX (electron diffraction X-ray) spectroscopy was coupled with SEM to identify the elemental composition. Morphologies of the prepared products were detected using a Philips EM208S transmission electron microscope (TEM; The Netherlands) at an accelerating voltage of 150 kV. To prepare TEM samples, a drop of the diluted latex was placed onto a copper grid and then left to dry at 30 °C for 15 min. Molecular weight and its distribution was determined in THF at a flow rate of 1 mL min^{-1} using a GPC Agilent 1100 (CA, USA) with a refractive index detector. Narrow PS standards were employed for calibrations. Nanoparticles were centrifuged, washed with fresh DI water and vacuum dried prior to dissolution in THF.

Magnetic properties of the samples were determined by vibrating sample magnetometer (VSM, model LBKFB, Kavir Magnet Co., Kashan, Iran). A small amount of powder was weighed and placed on the probe and the magnetic field was applied in perpendicular direction to the sample surface.

Sonication was carried out by means of an ultrasound generator, SONOPULS Ultrasonic homogenizer, Model HF-GM 2200 (BANDELIN Electronics GmbH and Co. KG, Berlin, Germany) and a titanium microtip KE-76 probe with 6 mm diameter was employed as the probe.

Table 1
Miniemulsion polymerization in preparation of MNP0-S0 latex.

Component	Amount
DI water (mL)	27
MMA (g)	3
KPS (g)	0.075
Triton X-100 (g)	0.124
SDS (g)	0.177
$NaHCO_3$ (g)	0.060
HD (g)	0.075

Table 2
Composition of the samples with various amounts of m-Fe_3O_4 NPs and SPEA.

Sample	m-Fe_3O_4 NPs (g)	SPEA (g)	m-Fe_3O_4 NPs (wt%)[a]	SPEA (wt%)[a]
MNP0-S0	0	0	0	0
MNP1-S0	0.03	0	1	0
MNP2-S0	0.06	0	2	0
MNP0-S1	0	0.03	0	1
MNP0-S2	0	0.06	0	2
MNP1-S1	0.03	0.03	1	1
MNP1-S2	0.03	0.06	1	2
MNP1-S3	0.03	0.09	1	3
MNP2-S2	0.06	0.06	2	2

[a] Relative to MMA amount.

3. Results and discussion

Photochromic properties and isomerization rate of SPEA depend on its interaction with the surrounding environment, e.g. chemical structure, solvent characteristics and pH [4,43]. For photochromic-magnetic polymer nanoparticles, there is no information available in the literature about these interactions with magnetic field of the nanoparticles and any attempt in this area will be worthwhile.

Here, superparamagnetic Fe_3O_4 NPs were synthesized through thermal decomposition method and chemical modification of their surface was carried out with 3-(trimethoxysilyl) propyl methacrylate (MPS). Emulsion-based systems are among the most effective procedures for preparation of multifunctional polymer nanoparticles. PMNPs containing MMA, SP groups and m-Fe_3O_4 NPs were prepared via miniemulsion polymerization, through which m-Fe_3O_4 NPs were designed to locate in the core and poly (MMA-co-SPEA) in the shell (Scheme 1). The simultaneous presence of SP groups and m-Fe_3O_4 NPs in the polymeric composite nanoparticles will provide photochromic and magnetic properties, respectively. This strategy will guarantee preventing of some disadvantages regarding to each segment, such as dye leakage or aggregation, irreversible oxidation of Fe_3O_4 NPs, easy processability, tailoring the switchability plus bio- and solvent-compatibility.

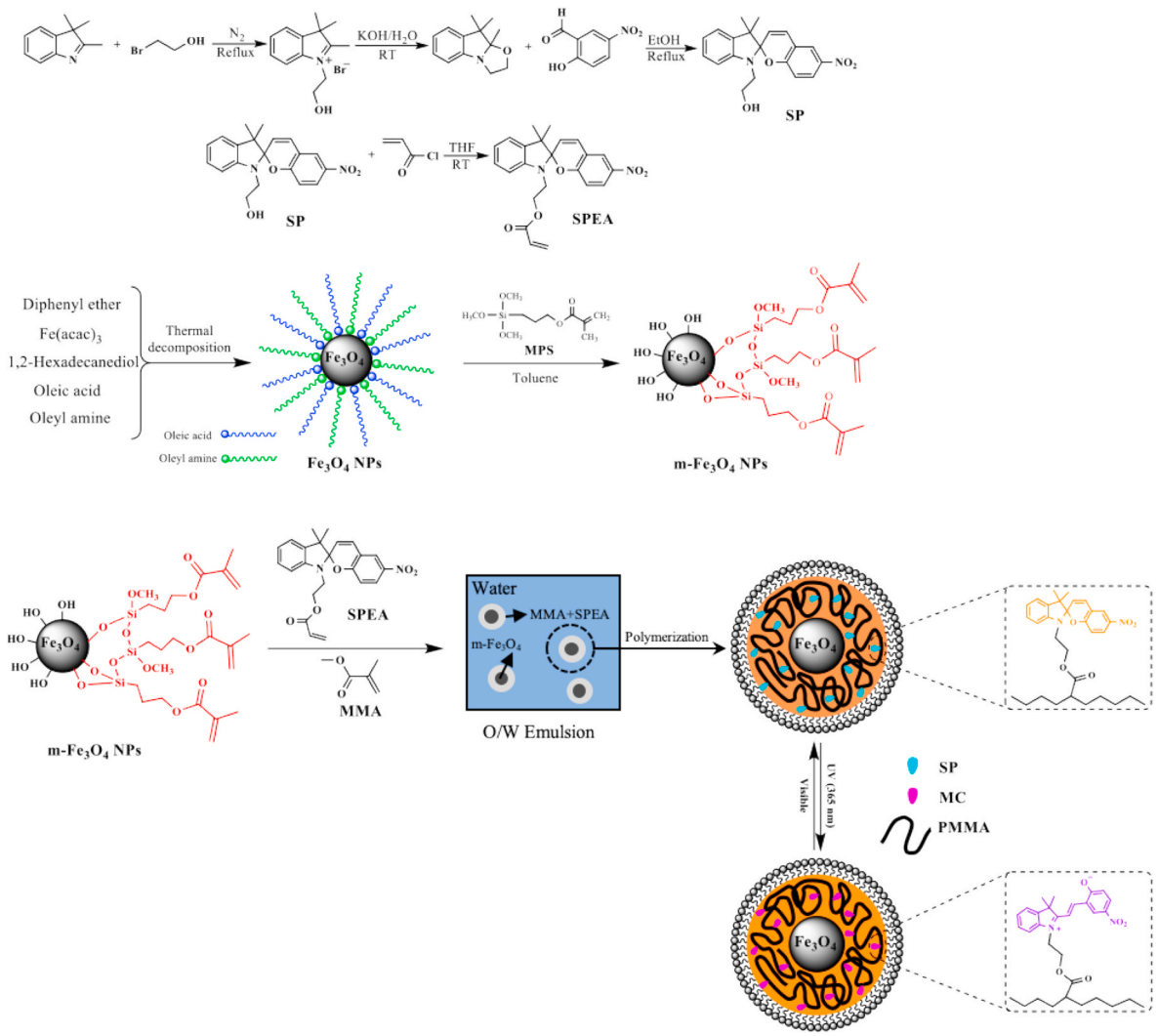

Scheme 1. Preparation of SPEA (up), superparamagnetic Fe_3O_4 NPs plus their surface modification (middle), and miniemulsion polymerization with MMA and SPEA (below). SP⇄MC isomerization under UV (365 nm) and visible irradiations has been shown in the bottom.

3.1. Preparation and surface modification of the magnetite nanoparticles

Preparation of SPIONs was performed through thermal decomposition method in order to achieve a good control on their both size and size distribution with fine dispersion in the organic medium. Crystalline structure of the prepared Fe_3O_4 NPs was identified by XRD analysis (Fig. 1S, Supporting Information). The characteristic peaks in the XRD pattern of Fe_3O_4 NPs show a cubic spinel structure. The strong six discrete peaks at 2θ of 30.6°, 36.4°, 43.3°, 53.4°, 56.9° and 63.1° refer to the lattice planes of [220], [311], [400], [422], [511] and [440], respectively, with no impurity in Fe_3O_4 NPs. All diffraction peaks in the XRD pattern comply with the characteristic diffractions of standard Fe_3O_4 NPs inverse spinel structure (Joint Committee for Powder Diffraction Studies, JCPDS, Card No. 19–0629). Average size of the

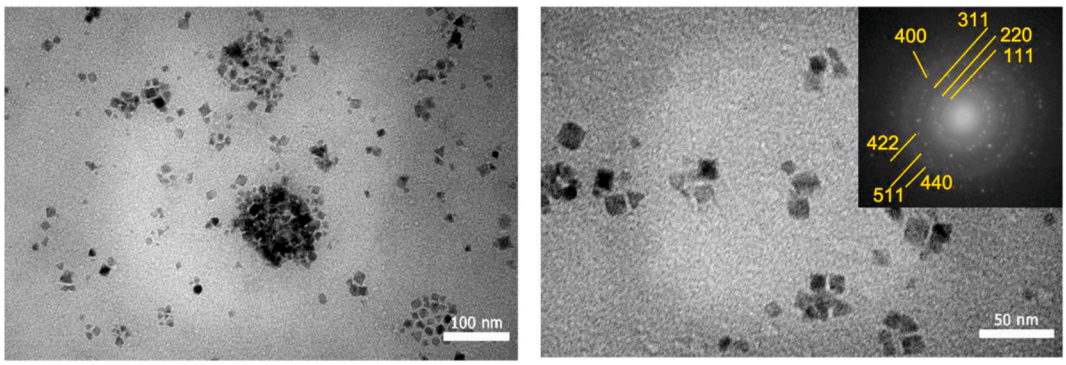

Fig. 1. TEM micrographs of the prepared Fe_3O_4 cubic magnetic nanoparticles with different magnifications. The inset represents SAED pattern of the magnetite with assigned lattice indexes.

prepared Fe_3O_4 NPs crystallite was estimated from XRD results, using Scherrer's equation [24] and it was found 11 nm.

Morphology and size of the obtained Fe_3O_4 NPs were investigated by TEM and the images are shown in Fig. 1. It can be seen that the particles possess almost cubic shape with regular distribution and size of about 15 nm. SAED (selected area electron diffraction) pattern from TEM image is in accordance with the recorded XRD pattern too. Hence and according to the small size and shape of the particles, it is expected to have excellent superparamagnetic properties.

FT-IR spectra of Fe_3O_4 NPs and m-Fe_3O_4 NPs were taken (Fig. 2S, Supporting Information). The characteristic peaks at 443 and 588 cm^{-1} belong to the stretching vibration of Fe^{3+}–O and Fe^{2+}–O bonds, respectively. The bands at 3440 and 1625 cm^{-1} (merged with C═C bond) correspond to O–H stretching and bending vibrations respectively, and confirming the synthesis of Fe_3O_4 NPs. The peaks at 1406 (sym) and 1565 (*asym*) cm^{-1} are related to the stretching vibration of $–COO^-$ bond from the added oleic acid (Fig. 2Sa). The bands appeared at 1108, 1460, 1540, 2850 and 2920 cm^{-1} are attributed to C–N (stretching), CH_2 (bending), NH_2 (bending) and aliphatic C–H (sym and *asym*), respectively, due to the presence of oleylamine on the surface of Fe_3O_4 NPs [44]. The presence of MPS moieties on the surface of Fe_3O_4 NPs was confirmed by FT-IR spectrum of m-Fe_3O_4 NPs (Fig. 2Sb). The appearance of new peaks at 802 cm^{-1} (Si–O–Si bending), 1013 cm^{-1} (Si–O–Si symmetric stretching), 1095 cm^{-1} (Si–O–Si asymmetric stretching), 1170 cm^{-1} (C–O stretching), 1260 cm^{-1} (Si–C stretching), 1455 cm^{-1} (C–H bending), 1637 cm^{-1} (C═C stretching) and 1717 cm^{-1} (C═O stretching) implies successful chemically surface modification of magnetite NPs with MPS.

Energy dispersive X-ray (EDX) analysis as well as the corresponding elemental map for Si and Fe were carried out to confirm the co-existence of MPS and Fe_3O_4 NPs too (Fig. 3S, Supporting Information). EDX pattern shows the existence of Si (3.51 wt%), C (11.43 wt%), O (34.36 wt%) and Fe (50.70 wt%), depicting the inclusion of MPS on the surface of Fe_3O_4 NPs. However, Si- and Fe-mapping reveal uniform distribution of the components.

Magnetic properties of Fe_3O_4 NPs and m-Fe_3O_4 NPs were evaluated by vibrating sample magnetometer (VSM) analysis (Fig. 2). The values of M_s (saturation magnetization), M_r (remanence magnetization), H_c (coercive force) and M_r/M_s for the prepared samples were extracted from VSM analysis and summarized in Table 3. High M_s, low M_r and low H_c values and also approaching of M_r/M_s to zero are good indications for obtaining SPIONs with magnetic single domains here. These illustrate that both samples have no hysteresis loop. Also, M_s value of m-Fe_3O_4 NPs (56.42 emu/g) did not significantly reduce in comparison with that of Fe_3O_4 NPs (58.05 emu/g), implying that the crystalline and magnetic domains have not been influenced during this modification reaction.

3.2. Particle size and morphology of PMNPs

To achieve suitable photochromic properties, particles size in the latexes must necessarily be smaller than half of the incident beam wavelength and usually below 100 nm [11]. Here, all affecting parameters except SPEA concentration and m-Fe_3O_4 NPs content were kept constant in the recipes.

Average particles size (D_z) and polydispersity index (PDI) of the prepared latexes were determined by dynamic light scattering (DLS) analysis and their zeta potentials were also measured (Fig. 3). The obtained particles sizes were all laid in the range of 65–95 nm. It could be found that D_z of the samples did not change significantly by increasing the number of m-Fe_3O_4 NPs in the polymerization recipe. Similarly, no obvious variation in D_z was found with the increase in SPEA concentration at constant m-Fe_3O_4 NPs content. These results illustrate that the considered amounts of SPEA and modified magnetite nanoparticles did not affect the polymerization process, particle formation and growth. On the other hand, the particles were all below 100 nm and the latexes had almost narrow particles size distributions (Table 4). It is expected that the presence of SPEA in the particles shell would cause some changes in

Table 3
Magnetic parameters from VSM analysis for the prepared Fe_3O_4 and m-Fe_3O_4 nanoparticles.

Sample	M_s (emu/g)	M_r (emu/g)	H_c (Oe)	M_r/M_s
Fe_3O_4 NPs	58.05	0.008	0.181	0.00014
m-Fe_3O_4 NPs	56.42	0.006	0.142	0.0001

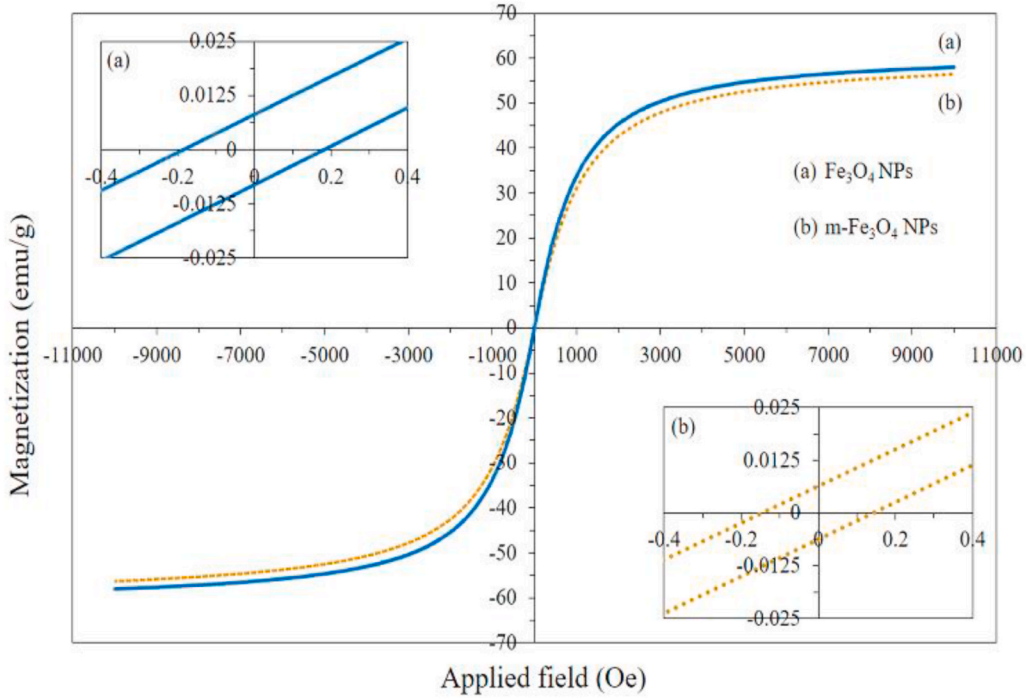

Fig. 2. VSM analysis for Fe_3O_4 (a) and m-Fe_3O_4 (b) nanoparticles. The insets reveal the corresponding expanded regions.

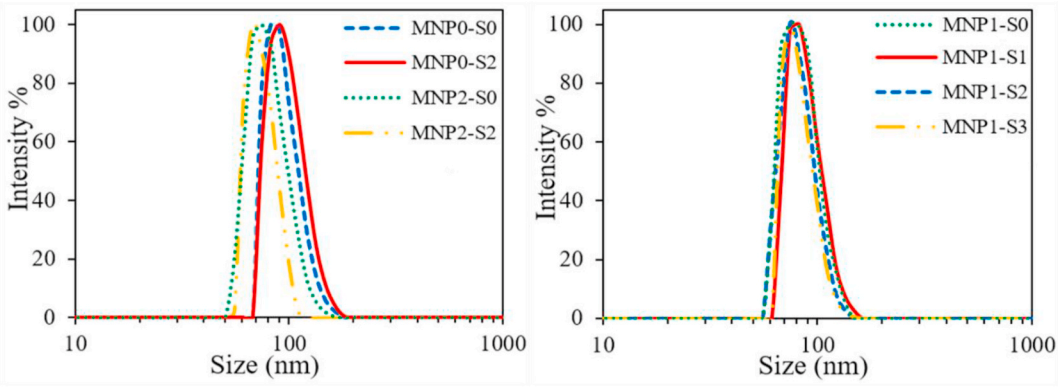

Fig. 3. DLS analysis of the prepared PMNPs with different SPEA concentrations and m-Fe_3O_4 NPs contents.

Table 4
Extracted data from DLS analysis for the prepared latexes.

Sample	MNP0-S0	MNP0-S2	MNP2-S0	MNP2-S2	MNP1-S0	MNP1-S1	MNP1-S2	MNP1-S3	MNP1-S2 (after UV)
Dz (nm)	88	93	80	69	86	83	78	76	–
PDI	0.187	0204	0.225	0.156	0.191	0.172	0.179	0.164	–
Zeta Potential (mV)	−37.14	−25.82	–	–	–	−27.69	−26.03	−24.23	−20.73

their surface properties, especially after UV irradiation. Zeta potential measurements were used to verify this, and the results for some typical samples have been given in Table 4.

Due to the presence of SDS as the anionic surfactant, negative zeta potentials are predictable. It should be noted that the amount of SDS in all PMNPs samples is identical. However, zeta potential of PMNPs

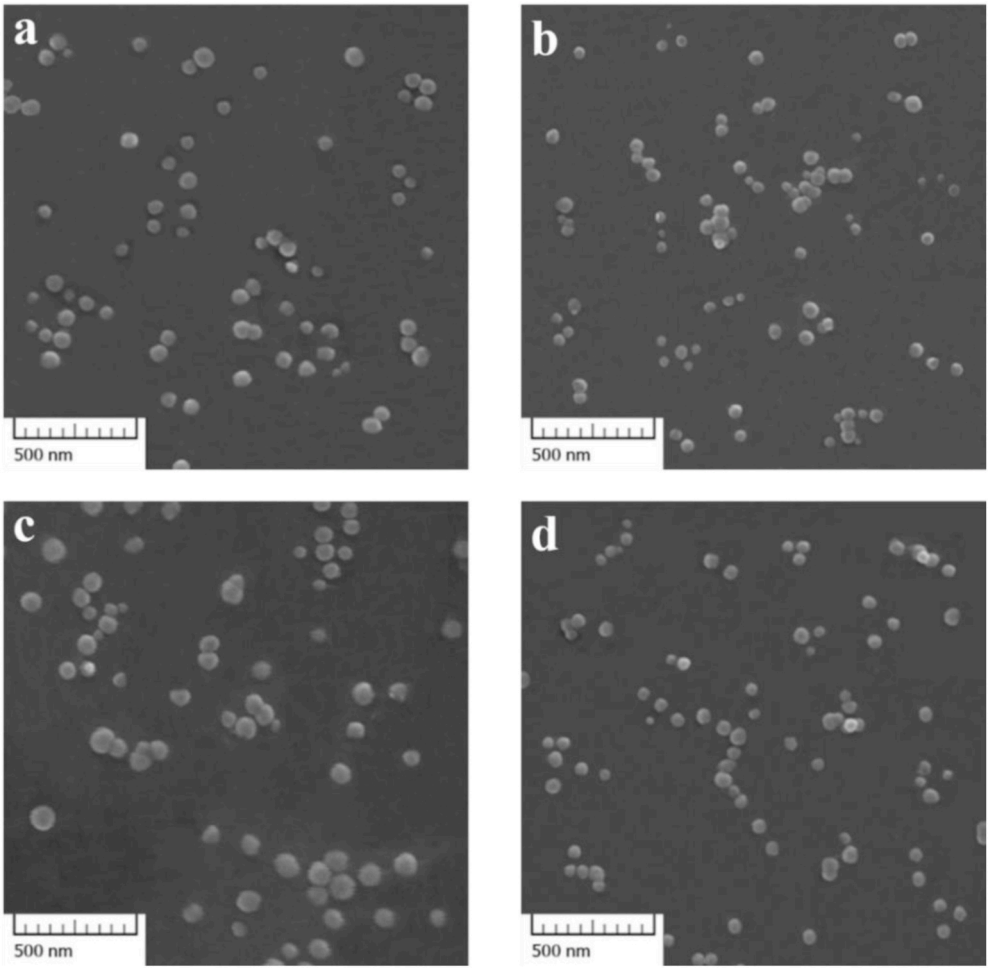

Fig. 4. SEM micrographs of (a) MNP0-S0, (b) MNP2-S0, (c) MNP0-S2 and (d) MNP1-S2 latex particles.

increased by the increase in SPEA content slightly. This could be attributed to the localization of SPEA on the particles surface, which suppresses the negative charge density with approximately similar sizes in PMNPs. This was strictly approved by measurement of zeta potential of MNP1-S2 after UV irradiation at 365 nm typically. Zeta potential is expected to change after UV irradiation due to the conversion of SP to MC with zwitterionic character, and this was found by the increase from −26.03 to −20.73 mV, revealing the variation in charge density around PMNPs after MC formation. On the other hand, this analysis for MNP0-S2 and MNP1-S2 showed no significant changes with respect to the engulfment of m-Fe_3O_4 NPs inside PMNPs and their entrapment by the copolymer shell.

As a complementary characterization, MNP0-S0 (as a test sample that had similar polymerization recipe without any insoluble Fe_3O_4 NPs) was chosen for GPC analysis to measure molecular weights of the copolymer and their distribution (Fig. 4S, Supporting Information). The obtained weight and number average molecular weights were found 1.85×10^5 and 7.2×10^4 g mol^{-1}, respectively, with PDI of 2.6.

SEM and TEM analyses were used to investigate the morphology and particle size of the obtained latex particles. Fig. 4 demonstrates that the obtained particles are spherical and their sizes are in good agreement with DLS results.

TEM image of MNP1-S2 has been shown in Fig. 5 typically. It is evident that magnetite NPs have been located inside the polymer particles and the predicted core-shell morphology is obvious. No extra ring was observed in SAED pattern of the prepared nanocomposite nanoparticles, implying negligible amount of silica. The approximate amount of Fe_3O_4 NPs was estimated in the range of 1.5–2 wt% by TGA analysis of the prepared nanocomposite samples (Fig. 5S, Supporting Information) with respect to the applied procedure. Totally, DLS, SEM and TEM analyses are all consistent and confirm the spherical core-shell morphology of the latex nanoparticles with average sizes below 100 nm with encapsulated multiple m-Fe_3O_4 NPs.

3.3. Study on the interaction between photochromic and magnetic components

After approving the structural characteristics of the obtained PMNPs, the possible interactions between magnetite nanoparticles and photochromic moieties were studied for the first time. For this reason, photochromic properties of the latexes (0.5 wt%) were assessed by UV–Vis analysis (Fig. 6). UV irradiation causes isomerization of the closed ring and nonpolar form of SP (colorless) into the open form and zwitterionic merocyanine (colored) together with color changes in the latex. This will result in appearance of strong absorption bands in the ranges of 350–450 and 450–650 nm with maximum absorption wavelength (λ_{max}) at 388 nm and 570 nm. SPEA aqueous solution was exposed to UV irradiation and its UV spectra has been shown in Fig. 7S (Supporting Information). The colorless SPEA was converted to the colored merocyanine form upon UV irradiation (365 nm), which could be identified by strong absorption bands in the ranges of 350–450 and 450–650 nm. All of the latex samples had almost similar λ_{max}s to SPEA at 388 and 570 nm, referring to SP⇄MC isomerization upon UV–Vis irradiation. Maximum absorbance (A_{max}) for each peak was measured and has been summarized in Table 5. By entrance of SP into the polymeric nanoparticles, λ_{max} for MC shifted from 514 to 570 nm ($\pi \rightarrow \pi^*$ electronic transition of the merocyanine form), while λ_{max} for $n \rightarrow \pi^*$ electronic transition of the chromene moiety (388 nm) did not change. This would be explained by the environmental effect of the polymeric matrix on stabilization of MC isomer and increase in conjugation length. All of the prepared latexes had favorable photochromic properties and were identifiable evidently (Fig. 6c). The presence of SP inside nanocomposite nanoparticles was also traced by XRD analysis typically for MNP1-S2 (Fig. 6S, Supporting Information), representing an extra peak at 2θ of 12.3° and the intensified peak at 15° relative to magnetite (Fig. 1S, Supporting Information). These two new peaks would be related to the presence of crystalline SP in the obtained nanocomposite nanoparticles.

The effects of increasing amounts of m-Fe_3O_4 NPs and SPEA on photochromic properties were studied, and it was found that the absorption intensity improved by the increase in magnetite content. As expected, A_{max} increased from MNP0-S1 to MNP0-S2 with the increase in SPEA content (Table 5), this was significantly observed for MNP1-S2 (104%) and MNP2-S2 (176%), while the amount of SPEA was kept constant in these samples (Fig. 6b). These notable variations in A_{max} values were accompanied by a slight red shift (5 nm in the corresponding λ_{max}s. This increment in the absorption intensity might originate from one or more triggers like enhanced light absorption by Fe_3O_4 NPs, stabilization of MC form in vicinity of Fe_3O_4 NPs and stacking of MC isomers. If stacking occurs, another absorption band at longer wavelengths of 570 nm (~620 nm) representing the formation of J-aggregates of MC isomers will be expected [42]. Due to the absence of new absorption band at longer wavelength, this phenomenon is less likely for observing such an enhancement in intensity by introducing magnetite. On the other hand, magnetite nanoparticles are able to strongly absorb light at a wide range of wavelength with a more preference in UV region (Fig. 8S, Supporting Information). This is the reason for detecting high absorption of UV irradiation beside the incorporated photochromic groups. There are also some reports on the enhanced light absorption by aggregates of magnetite nanoparticles which are consistent with the above findings [19,45]. Either enhancement in absorption intensity or a slight bathochromic shift in λ_{max} would be the result of possible stabilization of MC zwitterionic form with the vicinal Fe_3O_4 NPs through dipolar interactions, and also through dipole-magnetic interactions (with magnetic field of Fe_3O_4 NPs).

As a consequence, the coexistence and close contact of magnetite nanoparticles with photochromic moieties may provide high efficiency for the applications at which multi-responsivity accompanied by improved absorption intensity are specially demanded.

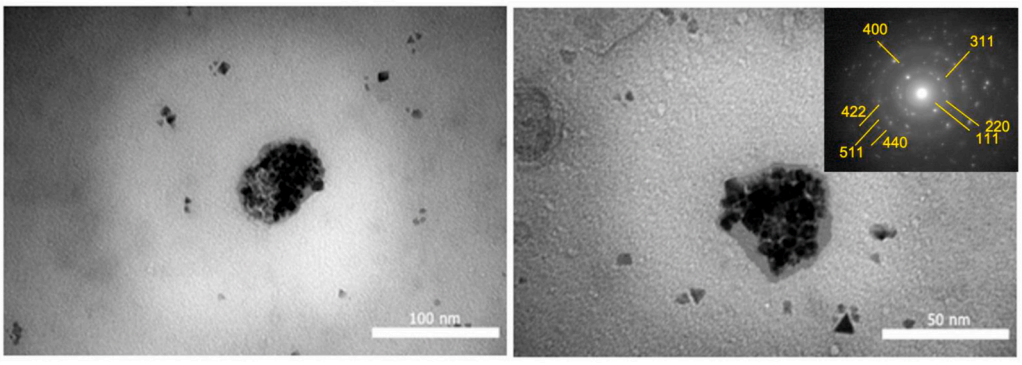

Fig. 5. TEM micrographs of MNP1-S2 with different magnifications. The dark region corresponds to the magnetite NPs and the grey region reveals the polymeric layer. The inset represents SAED pattern of the prepared nanocomposite particles.

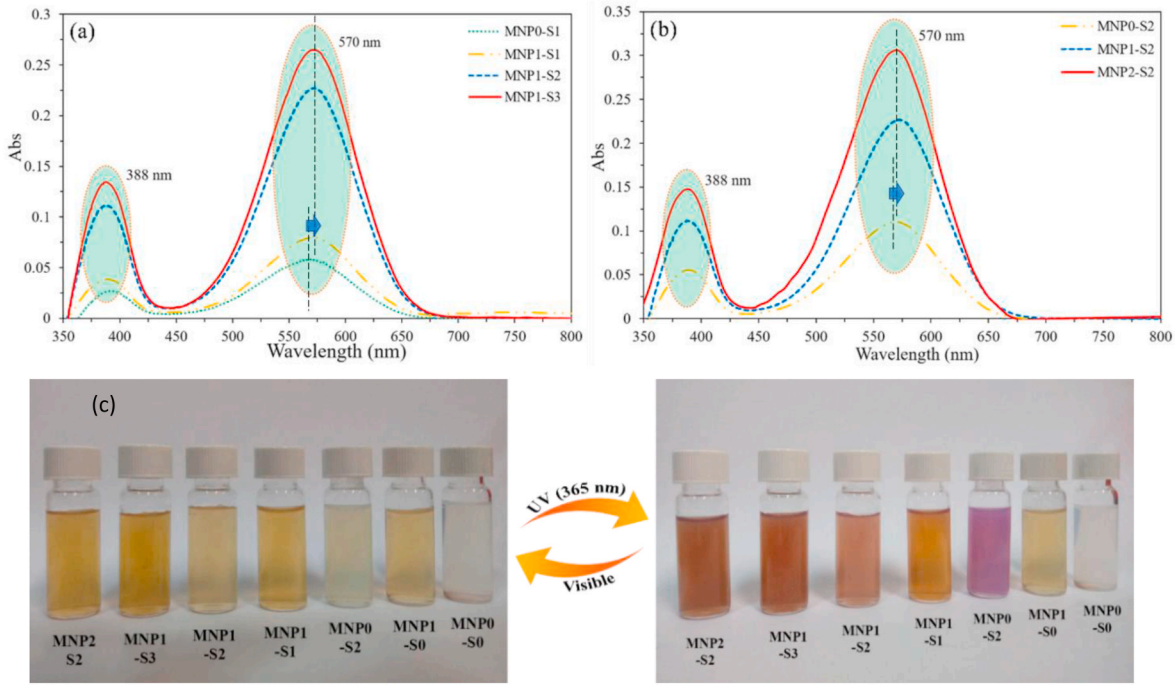

Fig. 6. UV–Vis spectra of the stimuli-responsive PMNPs containing different SPEA and m-Fe_3O_4 NPs ratios after UV illumination (365 nm, 5 min) (a and b). Color changes of the latexes (0.5 wt %) during SP ⇄ MC isomerization with UV and visible irradiations (c). (For interpretation of the references to color in this figure legend, the reader is referred to the Web version of this article.)

Table 5
The extracted numerical data from UV–Vis spectra.

Sample	A_{max} at 570 nm	A_{max} at 388 nm	Increment in A_{max} at 570 nm (%)	Increment in A_{max} at 388 nm (%)
MNP0-S1	0.056	0.028	–	–
MNP0-S2	0.111	0.056	98[a]	100[a]
MNP1-S1	0.080	0.039	42[a]	39[a]
MNP1-S2	0.227	0.110	305[a]/104[b]	293[a]/96[b]
MNP1-S3	0.265	0.135	373[a]	382[a]
MNP2-S2	0.306	0.148	446[a]/176[b]	429[a]/164[b]

[a] Increment in absorption intensity compared to MNP0-S1.
[b] Increment in absorption intensity compared to MNP0-S2.

With respect to the advantages of MNP1-S2 and MNP2-S2 samples, their magnetic behaviors were studied as well. As already shown, closely related magnetite NPs had synergistic effect on photochromic properties and enhanced absorption intensities together with a slight red shift in λ_{max}. To check whether this interaction is mutual, i.e. photoactivated moieties have any effect on the magnetic properties of the adjacent Fe_3O_4 NPs, VSM analysis was recorded for these two samples in the presence and absence of UV irradiation at 365 nm (Fig. 7). The results have been extracted and shown in Table 6. A slight change (4% for MNP1-S2) in magnetic parameters was found after exposure to UV (365 nm) for 5 min and this was more sensed for MNP2-S2 (10%) with higher Fe_3O_4 NPs content. This improvement is remarkable in comparison with previous reports, such as 0.1 emu.g^{-1} elevation upon 180 min UV irradiation (in the magnetic field of −3500 to +3500 Oe) [41] and also up to 5% increment in magnetization after 250 min UV irradiation [42].

It has been demonstrated that the photoisomerization alters the distance between Fe_3O_4 NPs or their coordination sphere, and these changes are reflected in M_s, M_r and H_c of the magnetite NPs [39,40,46]. In other words, SP to MC isomerization and in-situ formation of the zwitterionic MC form enhance magnetization of Fe_3O_4 NPs in prolonged UV irradiation without affecting superparamagnetic properties. There have recently been few reports on light-induced magnetization of molecular nanoparticles, including Prussian blue analogs, Hofmann-type systems, single-molecule magnets and those based on transition metal oxides like Fe_3O_4 [47,48]. These are in accordance with our observations and probable induced photo-magnetization of Fe_3O_4 NPs. Noteworthy that photo-magnetism is detectable at temperatures below the block temperature of nano magnetite. The presence of SP groups adjacent to Fe_3O_4 NPs may have shifted this process toward ambient temperature. On the other hand, anisotropic energy barrier of Fe_3O_4 NPs should be lowered in order to observe light-induced magnetization [48]. It seems that zwitterionic MC isomers have been able to reduce magnetic energy barrier for spin-flip transitions far more than what temperature reduction do and promote this photo-magnetism. Dipole moments of SP and MC are ~4–6 D and ~14–18 D, respectively [49,50]. MC isomer has quite different affinity to chemical compounds due to its higher polarity, and particularly to metal ions [51,52]. It could be concluded that the established efficient dipole-magnetic interaction and subsequent reduced magnetic energy barrier as a result of interaction between Fe cations and MC zwitterions are responsible for such observations. More detailed elucidation needs further complementary experiments which is not in the scope of the present work and we hope these may open up new ways for practical application of spin-based electronics and photonics.

3.4. Kinetic of isomerization

The kinetic of photoisomerization and variations in the absorption intensity of all latexes (0.5 wt%) in different time intervals upon UV irradiation have been demonstrated in Fig. 8. In order to inspect the effect of m-Fe_3O_4 NPs on switching rate of SP to MC (Fig. 8a–f) and reversible isomerization (Fig. 8e and f) after irradiations, the absorption intensities of MC form was measured at the corresponding λ_{max}s. All the samples attained their maximum absorption intensities under UV irradiation (365 nm) after about 60 s with a steep slope before reaching to

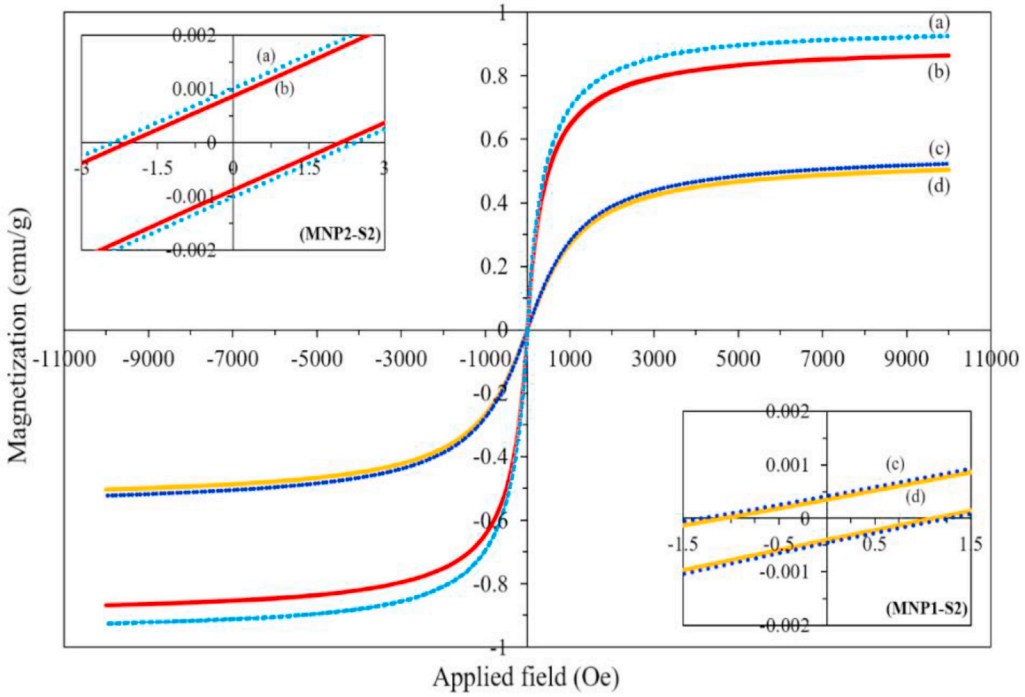

Fig. 7. VSM analyses of (a) MNP2-S2 (after UV), (b) MNP2-S2 (before UV), (c) MNP1-S2 (after UV) and (d) MNP1-S2 (before UV). The insets reveal the corresponding expanded regions and UV irradiation was carried out at 365 nm for 5 min.

Table 6
Magnetic parameters obtained from VSM analysis for MNP1-S2 and MNP2-S2 samples before and after UV irradiation at 365 nm (for 5 min).

Sample	Before exposure to UV irradiation				After exposure to UV irradiation				Variation upon UV exposure (%)			
	M_s (emu/g)	Mr (emu/g)	Hc (Oe)	Mr/Ms	Ms (emu/g)	Mr (emu/g)	Hc (Oe)	Mr/Ms	ΔMs (emu/g)	ΔMr (emu/g)	ΔHc (Oe)	ΔMr/Ms
MNP1-S2	0.5036	0.00026	1.154	0.0005	0.5238	0.00032	1.272	0.0006	4.0	23.1	10.2	20
MNP2-S2	0.8645	0.00088	2.103	0.0010	0.9552	0.00101	2.401	0.0011	10.5	14.8	14.2	10

the plateau region. The complete sweep cycle has been demonstrated in Fig. 8e and f in which, a direct correlation between the absorption intensity and UV irradiation time is clearly observed according to the formation of MC isomer. The results of absorption intensity show an exponential dependency of the isomerization rate on irradiation time in both directions (SP⇄MC) for MNP1-S2 and MNP2-S2 typically.

Totally, SP to MC isomerization kinetic for all latexes could be well-described by Equation (1), while that for MC to SP isomerization was fitted by Equation (2) and the later was studied for those in Fig. 8e and f. These equations are applicable to both λ_{max}s at 388 and 570 nm.

$$\frac{\text{Normalized absorbance (t)}}{\text{Normalized absorbance (0)}} = A - A' \exp(-k_C t) \quad \text{Eq 1}$$

$$\frac{\text{Normalized absorbance (t)}}{\text{Normalized absorbance (0)}} = A_\circ + A'' \exp(-k_D t) \quad \text{Eq 2}$$

where A, $A_\circ$, A' and A'' are constant values; k_C and k_D represent the rate constants for SP to MC (Equation (1)) and MC to SP (Equation (2)) photoisomerization upon UV and visible light irradiations, respectively. The normalized absorbance values are the maximum absorbance intensities of MC form in the photoresponsive latexes at 388 or 570 nm after UV or visible light irradiations at times t and 0.

It has previously been shown that polarity, pH of the environment and chain flexibility are the influential factors on isomerization kinetics of photoactive groups [4,17]. Here, the proposed interaction between magnetic field of Fe_3O_4 NPs and instantly produced dipole moments in MC isomers (by UV light) was followed by kinetic studies of the isomerization process as a new parameter beside the above factors. The effect of m-Fe_3O_4 NPs on the isomerization kinetic and photochromic properties was investigated for the samples with similar SPEA concentration in the polymer particles (MNP1-S2 and MNP2-S2). k_C or k_D and the absorption intensity are good indications to study the responsivity in such dual responsive latex particles during photoisomerization. Kinetic equations and the corresponding parameters, i.e. k_C, k_D, R^2 (coefficient of determination), and the required time to reach half of the final absorbance for color changes ($T_{1/2}$) have been extracted from Fig. 8 and summarized in Table 7. R^2 values depict good fitting of Equations (1) and (2) with the experimental results. It is worth mentioning that k_C or k_D and $T_{1/2}$ are approximately the same for each sample at both λ_{max}s (388 and 570 nm), depicting absorption consistency at these two wavelengths and formation of similar molecular structures in the presence and absence of m-Fe_3O_4 NPs. According to the obtained parameters for different samples in the presence of m-Fe_3O_4 NPs, maximum responsivity and minimum $T_{1/2}$ for SP to MC isomerization were observed for MNP2-S2. These illustrate that m-Fe_3O_4 NPs have got involved in the photoisomerization process and facilitated this process due to the enhanced light absorption. Coexistence of photochromic compound with magnetite nanoparticles not only led to facile formation of MC isomers, but also reduced the rate of reverse isomerization reaction (almost 50%) with respect to k_D and $T_{1/2}$ (about 40 s). The latter could be attributed to the stabilization of MC zwitterions through efficient interaction with Fe_3O_4 NPs lattices which has been discussed in previous section and its consequent less tendency toward interchange to SP form. Similarly, rapid SP to MC isomerization as well as slow MC to SP isomerization have previously been reported by changing in polarity of the media or pH, where MC isomer would become more stable [4].

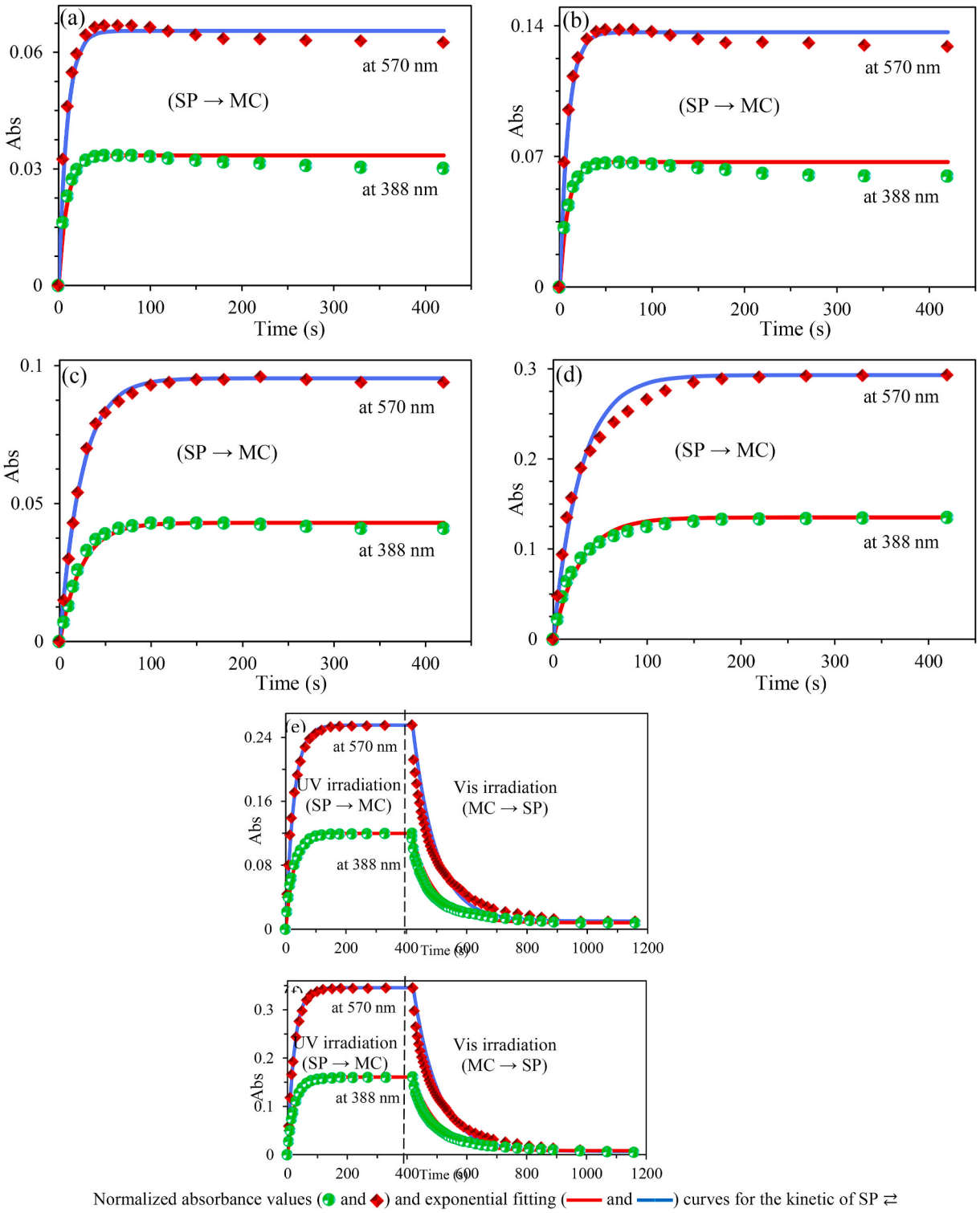

Fig. 8. Normalized absorbance values (and) and exponential fitting (and) curves for the kinetic of SP ⇄ MC isomerization of the prepared stimuli-responsive PMNPs latexes at the corresponding λ_{max}s under UV (365 nm) and visible irradiations: (a) MNP0-S1, (b) MNP0-S2, (c) MNP1-S1, (d) MNP1-S3, (e) MNP1-S2 and (f) MNP2-S2.

3.5. Photofatigue resistance and photo-switchability

Photoreversibility and photofatigue resistance of SPEA-containing latexes are important parameters in evaluation of the life-time and photochromic behavior in multi-responsive polymers. Here, the prepared diluted latex samples (0.5 wt%) were exposed to alternating illumination cycles of UV (365 nm, 5 min) and visible (5 min) lights during 9 cycles and the obtained absorption intensities were measured at 388 and 570 nm (Fig. 9). The absorbances were immediately measured after each irradiation within a 5 min interval between each cycle. This was carried out to analyze the role of incorporated Fe_3O_4 NPs on photofatigue resistance of SPEA. It had previously been approved that photoreversibility and photofatigue resistance of photochromic compounds are substantially boosted by inclusion into a hydrophobic

Table 7
Coloration and discoloration rate equations and the corresponding kinetic parameters for the prepared stimuli-responsive PMNPs latexes under UV (365 nm) and visible light irradiations for the samples containing various SPEA and m-Fe_3O_4 NPs ratios.

Isomerization	Sample	Absorbance at 388 nm					Absorbance at 570 nm				
		Equation	k_C (s^{-1})	k_D (s^{-1})	$T_{1/2}$ (s)	R^2	Equation	k_C (s^{-1})	k_D (s^{-1})	$T_{1/2}$ (s)	R^2
SP to MC	MNP0-S1	0.03346–0.03346 exp (-0.10625t)	0.10625	–	7	0.99	0.06553–0.06553 exp (-0.10631t)	0.10631	–	7	0.99
	MNP0-S2	0.06703–0.06703 exp (-0.10796t)	0.10796	–	6	0.99	0.13661–0.13661 exp (-0.10807t)	0.10807	–	6	0.99
	MNP1-S1	0.04302–0.04302 exp (-0.04187t)	0.04187	–	17	0.99	0.09541–0.09541 exp (-0.04193t)	0.04193	–	17	0.99
	MNP1-S2	0.11985–0.11985 exp (-0.03658t)	0.03658	–	19	0.99	0.25545–0.25545 exp (-0.03667t)	0.03667	–	19	0.99
	MNP1-S3	0.13502–0.13502 exp (-0.03451t)	0.03451	–	20	0.99	0.29312–0.29312 exp (-0.03461t)	0.03461	–	20	0.99
	MNP2-S2	0.16079–0.16079 exp (-0.04324t)	0.04324	–	16	0.99	0.34579–0.34579 exp (-0.04336t)	0.04336	–	16	0.99
MC to SP	MNP1-S2	0.00815 + 24.84378 exp (-0.01297t)	–	0.01297	53	0.99	0.01009 + 57.75152 exp (-0.01299t)	–	0.01299	53	0.99
	MNP2-S2	0.00841 + 23.16548 exp (-0.01195t)	–	0.01195	58	0.99	0.00724 + 52.04732 exp (-0.01198t)	–	0.01198	58	0.99

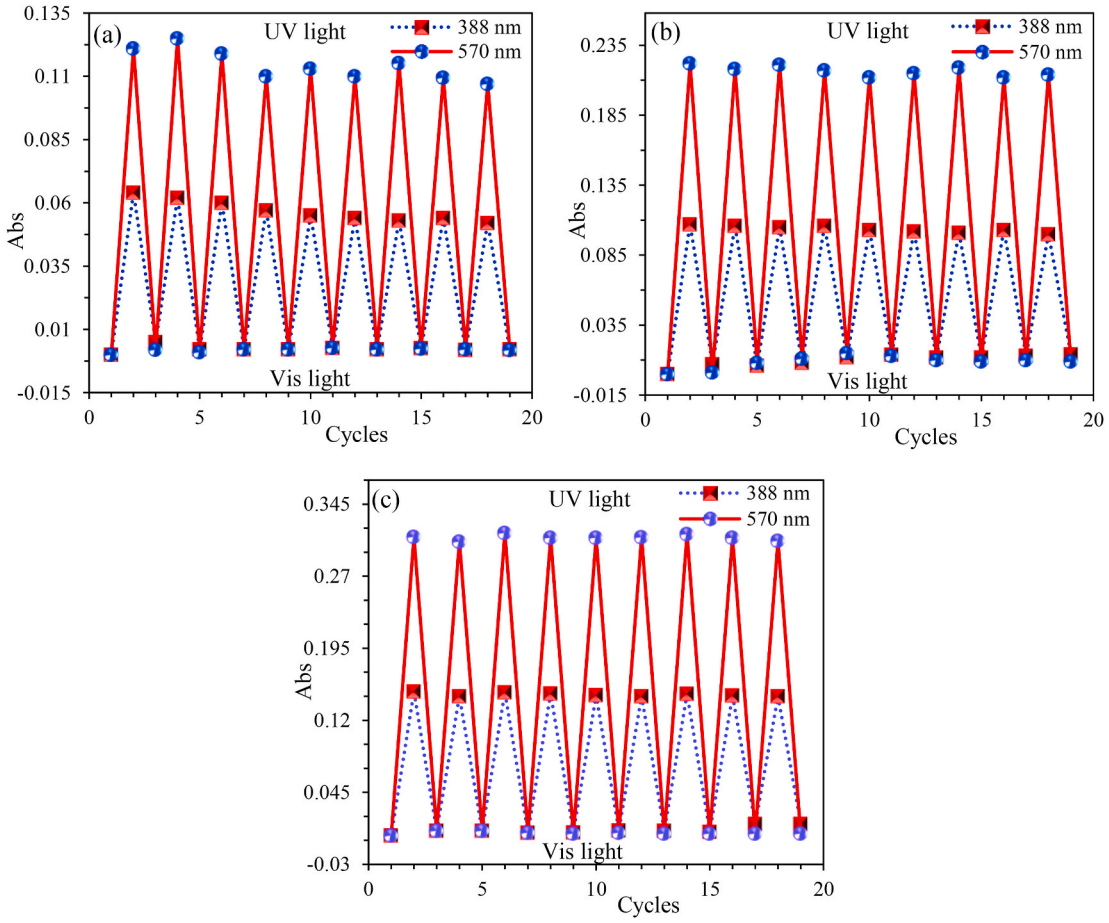

Fig. 9. Photofatigue resistance of the prepared stimuli-responsive PMNPs latexes upon alternating UV (365 nm, 5 min) and visible (5 min) irradiations: (a) MNP0-S2, (b) MNP1-S2 and (c) MNP2-S2.

polymeric matrix via covalent bonding [15]. Here, the obtained results exhibited excellent photostability and photoreversibility for the examined samples. It is evident from Fig. 9 that the internalized m-Fe_3O_4 NPs have caused significant enhancement in the photostability. Higher m-Fe_3O_4 NPs content in the sample made lower fluctuation of absorbance for the dual functional composite nanoparticles. It has already been reported that photofatigue resistance is controlled by the dose of absorbed light beside chemical stability of the photochromic compound [53]. Therefore, the observed steady absorbances in the presence of magnetite nanoparticles can be attributed to the enhanced contribution of Fe_3O_4 NPs in light absorption, resulting in limited fluctuations.

These confirm that such polymeric magnetic photoactive materials

may provide advanced characteristics for new applications in chemosensors, magnetic separation, targeted therapy, biomedical and biotechnology, bio-imaging and early diagnosis.

4. Conclusions

In this study, some novel, photochromic-magnetic polymer nanoparticles (PMNPs) were designed as efficient dual responsive probes via miniemulsion polymerization due to the presence of magnetite and spiropyran groups simultaneously. According to SEM, TEM and DLS analyses, all stimuli-responsive latex particles were spherical with sizes in the range of 65–95 nm. Zeta potential analysis revealed that SP groups in the prepared PMNPs have been localized in the outer layer. UV–Vis and VSM analyses were comprehensively followed to investigate probable mutual correlation between Fe_3O_4 NPs and MC form through magnetic field and dipolar interactions, because of their close interactions in each nanoparticle. The results showed that magnetic and photochromic properties had positive synergy and improved significantly. These were observed by measurement of magnetic parameters and UV absorptions intensities for several samples with various magnetite and SPEA contents. Studies on the kinetic of photoisomerization were another strong evidence to prove the above-mentioned effective interactions. However, photofatigue resistance and photo-switchability were improved for the prepared PMNPs with respect to those without Fe_3O_4 NPs.

This work represents a promising insight toward introducing new generation of multi-responsive materials for advanced applications such as chemosensors, magnetic separation, enhanced targeted therapy and simultaneous with bio-imaging for early diagnosis and magnetic triggered photo-switches.

Declaration of competing interest

This is also notable that there is no conflict of interest with this submission to Polymer.

Acknowledgement

We wish to express our gratitude to Iran Polymer and Petrochemical Institute (IPPI) for financial support of this work (Grant# 24761185).

Appendix A. Supplementary data

Supplementary data to this article can be found online at https://doi.org/10.1016/j.polymer.2021.123524.

References

[1] J. Keyvan Rad, A.R. Mahdavian, Preparation of fast photoresponsive cellulose and kinetic study of photoisomerization, J. Phys. Chem. C 120 (2016) 9985–9991, https://doi.org/10.1021/acs.jpcc.6b02594.

[2] S. Sanjabi, Z. Alinejad, A. Mouraki, A.R. Mahdavian, Controlled photoisomerization in acrylic copolymer nanoparticles based on spironaphthoxazine for reduced thermal reversion, Eur. Polym. J. 119 (2019) 487–498, https://doi.org/10.1016/j.eurpolymj.2019.07.019.

[3] B. Razavi, A. Abdollahi, H. Roghani-Mamaqani, M. Salami-Kalajahi, Light- and temperature-responsive micellar carriers prepared by spiropyran-initiated atom transfer polymerization: investigation of photochromism kinetics, responsivities, and controlled release of doxorubicin, Polymer 187 (2020), 122046, https://doi.org/10.1016/j.polymer.2019.122046.

[4] A. Abdollahi, A. Mouraki, M.H. Sharifian, A.R. Mahdavian, Photochromic properties of stimuli-responsive cellulosic papers modified by spiropyran-acrylic copolymer in reusable pH-sensors, Carbohydr. Polym. 200 (2018) 583–594, https://doi.org/10.1016/j.carbpol.2018.08.042.

[5] T. Ma, M. Walko, M. Lepoitevin, J.-M. Janot, E. Balanzat, A. Kocer, S. Balme, Combining light-gated and pH-responsive nanopore based on PEG-spiropyran functionalization, Adv. Mater. Interfaces 5 (2018), 1701051, https://doi.org/10.1002/admi.201701051.

[6] A. Radulescu, L.J. Fetters, D. Richter, Wax Crystal Control Nanocomposites Stimuli-Responsive Polymers, Springer Berlin Heidelberg, Berlin, Heidelberg, 2008, https://doi.org/10.1007/978-3-540-75500-5.

[7] J. Keyvan Rad, A.R. Mahdavian, S. Khoei, S. Shirvalilou, Enhanced photogeneration of reactive oxygen species and targeted photothermal therapy of C6 glioma brain cancer cells by folate-conjugated gold–photoactive polymer nanoparticles, ACS Appl. Mater. Interfaces 10 (2018) 19483–19493, https://doi.org/10.1021/acsami.8b05252.

[8] K. Parafiniuk, C. Monnereau, L. Sznitko, B. Mettra, M. Zelechowska, C. Andraud, A. Miniewicz, J. Mysliwiec, Distributed feedback lasing in amorphous polymers with covalently bonded fluorescent dyes: the influence of photoisomerization process, Macromolecules 50 (2017) 6164–6173, https://doi.org/10.1021/acs.macromol.7b00878.

[9] S. Kobatake, Y. Matsumoto, M. Irie, Conformational control of photochromic reactivity in a diarylethene single crystal, Angew. Chem. 117 (2005) 2186–2189, https://doi.org/10.1002/ange.200462426.

[10] J. Yin, G.-A. Yu, H. Tu, S.H. Liu, Novel photoswitching dithienylethenes with ferrocene units, Appl. Organomet. Chem. 20 (2006) 869–873, https://doi.org/10.1002/aoc.1144.

[11] A. Abdollahi, A.R. Mahdavian, H. Salehi-Mobarakeh, Preparation of stimuli-responsive functionalized latex nanoparticles: the effect of spiropyran concentration on size and photochromic properties, Langmuir 31 (2015) 10672–10682, https://doi.org/10.1021/acs.langmuir.5b02612.

[12] F. Khakzad, A.R. Mahdavian, H. Salehi-Mobarakeh, M.H. Sharifian, A step-wise self-assembly approach in preparation of multi-responsive poly(styrene-co-methyl methacrylate) nanoparticles containing spiropyran, J. Colloid Interface Sci. 515 (2018) 58–69, https://doi.org/10.1016/j.jcis.2018.01.012.

[13] F. Jiang, S. Chen, Z. Cao, G. Wang, A photo, temperature, and pH responsive spiropyran-functionalized polymer: synthesis, self-assembly and controlled release, Polymer 83 (2016) 85–91, https://doi.org/10.1016/j.polymer.2015.12.027.

[14] F. Khakzad, A.R. Mahdavian, H. Salehi-Mobarakeh, A. Rezaee Shirin-Abadi, M. Cunningham, Redispersible PMMA latex nanoparticles containing spiropyran with photo-, pH- and CO 2 - responsivity, Polymer 101 (2016) 274–283, https://doi.org/10.1016/j.polymer.2016.08.073.

[15] A. Abdollahi, Z. Alinejad, A.R. Mahdavian, Facile and fast photosensing of polarity by stimuli-responsive materials based on spiropyran for reusable sensors: a physico-chemical study on the interactions, J. Mater. Chem. C. 5 (2017) 6588–6600, https://doi.org/10.1039/C7TC02232H.

[16] A. Dunne, C. Delaney, A. McKeon, P. Nesterenko, B. Paull, F. Benito-Lopez, D. Diamond, L. Florea, Micro-capillary coatings based on spiropyran polymeric brushes for metal ion binding, detection, and release in continuous flow, Sensors 18 (2018) 1083, https://doi.org/10.3390/s18041083.

[17] M.H. Sharifian, A.R. Mahdavian, H. Salehi-Mobarakeh, Effects of chain parameters on kinetics of photochromism in acrylic–spiropyran copolymer nanoparticles and their reversible optical data storage, Langmuir 33 (2017) 8023–8031, https://doi.org/10.1021/acs.langmuir.7b01869.

[18] J.K. Rad, A.R. Mahdavian, H. Salehi-mobarakeh, A. Abdollahi, FRET phenomenon in photoreversible dual-color fluorescent polymeric nanoparticles based on azocarbazole/spiropyran derivatives. https://doi.org/10.1021/acs.macromol.5b02401, 2016.

[19] T.-T.D. Pham, Y.H. Seo, D. Lee, J. Noh, J. Chae, E. Kang, J. Park, T.J. Shin, S. Kim, J. Park, Ordered assemblies of Fe3O4 and a donor-acceptor-type π-conjugated polymer in nanoparticles for enhanced photoacoustic and magnetic effects, Polymer 161 (2019) 205–213, https://doi.org/10.1016/j.polymer.2018.12.020.

[20] A. Muela, D. Muñoz, R. Martín-Rodríguez, I. Orue, E. Garaio, A. Abad Díaz de Cerio, J. Alonso, J.Á. García, M.L. Fdez-Gubieda, Optimal parameters for hyperthermia treatment using biomineralized magnetite nanoparticles: theoretical and experimental approach, J. Phys. Chem. C 120 (2016) 24437–24448, https://doi.org/10.1021/acs.jpcc.6b07321.

[21] D. Shi, M.E. Sadat, A.W. Dunn, D.B. Mast, Photo-fluorescent and magnetic properties of iron oxide nanoparticles for biomedical applications, Nanoscale 7 (2015) 8209–8232, https://doi.org/10.1039/C5NR01538C.

[22] Z. Yu, C. Zhang, Z. Zheng, L. Hu, X. Li, Z. Yang, C. Ma, G. Zeng, Enhancing phosphate adsorption capacity of SDS-based magnetite by surface modification of citric acid, Appl. Surf. Sci. 403 (2017) 413–425, https://doi.org/10.1016/j.apsusc.2017.01.163.

[23] M. Arslan, T.N. Gevrek, J. Lyskawa, S. Szunerits, R. Boukherroub, R. Sanyal, P. Woisel, A. Sanyal, Bioinspired anchorable thiol-reactive polymers: synthesis and applications toward surface functionalization of magnetic nanoparticles, Macromolecules 47 (2014) 5124–5134, https://doi.org/10.1021/ma500693f.

[24] Y. Yang, A.R. Mahdavian, E.S. Daniels, A. Klein, M.S. El-Aasser, Gold deposition on Fe 3 O 4/(co)Poly(N -octadecyl methacrylate) hybrid particles to obtain nanocomposites with ternary intrinsic features, J. Appl. Polym. Sci. 127 (2013) 3768–3777, https://doi.org/10.1002/app.37647.

[25] K. Woo, J. Hong, S. Choi, H.-W. Lee, J.-P. Ahn, C.S. Kim, S.W. Lee, Easy synthesis and magnetic properties of iron oxide nanoparticles, Chem. Mater. 16 (2004) 2814–2818, https://doi.org/10.1021/cm049552x.

[26] A. Mouraki, Z. Alinejad, S. Sanjabi, A.R. Mahdavian, Anisotropic magnetite nanoclusters with enhanced magnetization as an efficient ferrofluid in mass transfer and liquid hyperthermia, New J. Chem. 43 (2019) 8044–8051, https://doi.org/10.1039/C9NJ00212J.

[27] A. Mahdieh, A.R. Mahdavian, H. Salehi-Mobarakeh, Chemical modification of magnetite nanoparticles and preparation of acrylic-base magnetic nanocomposite particles via miniemulsion polymerization, J. Magn. Magn Mater. 426 (2017) 230–238, https://doi.org/10.1016/j.jmmm.2016.11.091.

[28] L. Jiang, X. Zhou, G. Wei, X. Lu, W. Wei, J. Qiu, Preparation and characterization of poly(glycidyl methacrylate)-grafted magnetic nanoparticles: effects of the precursor concentration on polyol synthesis of Fe3O4 and [PMDETA]0/[CuBr2]

0 ratios on SI-AGET ATRP, Appl. Surf. Sci. 357 (2015) 1619–1624, https://doi.org/10.1016/j.apsusc.2015.10.044.
[29] R. Abu-Much, A. Gedanken, Sonochemical synthesis under a magnetic field: structuring magnetite nanoparticles and the destabilization of a colloidal magnetic aqueous solution under a magnetic field, J. Phys. Chem. C 112 (2008) 35–42, https://doi.org/10.1021/jp075637k.
[30] A.S. Drozdov, O.E. Shapovalova, V. Ivanovski, D. Avnir, V.V. Vinogradov, Entrapment of enzymes within sol–gel-derived magnetite, Chem. Mater. 28 (2016) 2248–2253, https://doi.org/10.1021/acs.chemmater.6b00193.
[31] R. Hufschmid, H. Arami, R.M. Ferguson, M. Gonzales, E. Teeman, L.N. Brush, N. D. Browning, K.M. Krishnan, Synthesis of phase-pure and monodisperse iron oxide nanoparticles by thermal decomposition, Nanoscale 7 (2015) 11142–11154, https://doi.org/10.1039/C5NR01651G.
[32] L. Qiao, Z. Fu, J. Li, J. Ghosen, M. Zeng, J. Stebbins, P.N. Prasad, M.T. Swihart, Standardizing size- and shape-controlled synthesis of monodisperse magnetite (Fe3O4) nanocrystals by identifying and exploiting effects of organic impurities, ACS Nano 11 (2017) 6370–6381, https://doi.org/10.1021/acsnano.7b02752.
[33] K.R. Reddy, W. Park, B.C. Sin, J. Noh, Y. Lee, Synthesis of electrically conductive and superparamagnetic monodispersed iron oxide-conjugated polymer composite nanoparticles by in situ chemical oxidative polymerization, J. Colloid Interface Sci. 335 (2009) 34–39, https://doi.org/10.1016/j.jcis.2009.02.068.
[34] K.R. Reddy, K.-P. Lee, A.I. Gopalan, Novel electrically conductive and ferromagnetic composites of poly(aniline-co-aminonaphthalenesulfonic acid) with iron oxide nanoparticles: synthesis and characterization, J. Appl. Polym. Sci. 106 (2007) 1181–1191, https://doi.org/10.1002/app.26601.
[35] S. Kango, S. Kalia, A. Celli, J. Njuguna, Y. Habibi, R. Kumar, Surface modification of inorganic nanoparticles for development of organic–inorganic nanocomposites—a review, Prog. Polym. Sci. 38 (2013) 1232–1261, https://doi.org/10.1016/j.progpolymsci.2013.02.003.
[36] Y. Wei, Q. Zeng, S. Bai, M. Wang, L. Wang, Nanosized difunctional photo responsive magnetic imprinting polymer for electrochemically monitored light-driven paracetamol extraction, ACS Appl. Mater. Interfaces 9 (2017) 44114–44123, https://doi.org/10.1021/acsami.7b14772.
[37] R. Di Corato, G. Béalle, J. Kolosnjaj-Tabi, A. Espinosa, O. Clément, A.K.A. Silva, C. Ménager, C. Wilhelm, Combining magnetic hyperthermia and photodynamic therapy for tumor ablation with photoresponsive magnetic liposomes, ACS Nano 9 (2015) 2904–2916, https://doi.org/10.1021/nn506949t.
[38] S. Karthik, N. Puvvada, B.N.P. Kumar, S. Rajput, A. Pathak, M. Mandal, N.D. P. Singh, Photoresponsive coumarin-tethered multifunctional magnetic nanoparticles for release of anticancer drug, ACS Appl. Mater. Interfaces 5 (2013) 5232–5238, https://doi.org/10.1021/am401059k.
[39] Y. Gong, J. Dai, H. Li, X. Wang, H. Xiong, Q. Zhang, P. Li, C. Yi, Z. Xu, H. Xu, P. K. Chu, Magnetic, fluorescent, and thermo-responsive poly(MMA-NIPAM-Tb(AA) 3 Phen)/Fe 3 O 4 multifunctional nanospheres prepared by emulsifier-free emulsion polymerization, J. Biomater. Appl. 30 (2015) 201–211, https://doi.org/10.1177/0885328215575761.
[40] E.A. Osborne, B.R. Jarrett, C. Tu, A.Y. Louie, Modulation of T2 relaxation time by light-induced, reversible aggregation of magnetic nanoparticles, J. Am. Chem. Soc. 132 (2010) 5934–5935, https://doi.org/10.1021/ja100254m.
[41] M. Taguchi, G. Li, Z. Gu, O. Sato, Y. Einaga, Magnetic vesicles of amphiphilic spiropyran containing iron oxide particles on a solid state substrate, Chem. Mater. 15 (2003) 4756–4760, https://doi.org/10.1021/cm0344515.
[42] Y. Einaga, M. Taguchi, G. Li, T. Akitsu, Z. Gu, T. Sugai, O. Sato, Magnetization increase of iron oxide by photoinduced aggregation of spiropyran, Chem. Mater. 15 (2003) 8–10, https://doi.org/10.1021/cm025648k.
[43] A. Abdollahi, J.K. Rad, A.R. Mahdavian, Stimuli-responsive cellulose modified by epoxy-functionalized polymer nanoparticles with photochromic and solvatochromic properties, Carbohydr. Polym. 150 (2016) 131–138, https://doi.org/10.1016/j.carbpol.2016.05.009.
[44] T.A. Lastovina, A.P. Budnyk, M.A. Soldatov, Y.V. Rusalev, A.A. Guda, A.S. Bogdan, A.V. Soldatov, Microwave-assisted synthesis of magnetic iron oxide nanoparticles in oleylamine–oleic acid solutions, Mendeleev Commun. 27 (2017) 487–489, https://doi.org/10.1016/j.mencom.2017.09.019.
[45] S. Fowler, J. Jiao, Analysis of light absorption by magnetite core in magnetically recoverable photocatalyst nanoparticles, Microsc. Microanal. 18 (2012) 1432–1433, https://doi.org/10.1017/S1431927612009014.
[46] G. Abellán, H. García, C.J. Gómez-García, A. Ribera, Photochemical behavior in azobenzene having acidic groups. Preparation of magnetic photoresponsive gels, J. Photochem. Photobiol. Chem. 217 (2011) 157–163, https://doi.org/10.1016/j.jphotochem.2010.10.003.
[47] T. Naito, T. Karasudani, K. Ohara, T. Takano, Y. Takahashi, T. Inabe, K. Furukawa, T. Nakamura, Simultaneous control of carriers and localized spins with light in organic materials, Adv. Mater. 24 (2012) 6153–6157, https://doi.org/10.1002/adma.201203153.
[48] S. He, J.S. DuChene, J. Qiu, A.A. Puretzky, Z. Gai, W.D. Wei, Persistent photomagnetism in superparamagnetic iron oxide nanoparticles, Adv. Electron. Mater. 4 (2018), 1700661, https://doi.org/10.1002/aelm.201700661.
[49] M.A. Gerkman, S. Yuan, P. Duan, J. Taufan, K. Schmidt-Rohr, G.G.D. Han, Phase transition of spiropyrans: impact of isomerization dynamics at high temperatures, Chem. Commun. 55 (2019) 5813–5816, https://doi.org/10.1039/C9CC02141H.
[50] Q. Shen, Y. Cao, S. Liu, M.L. Steigerwald, X. Guo, Conformation-induced electrostatic gating of the conduction of spiropyran-coated organic thin-film transistors, J. Phys. Chem. C 113 (2009) 10807–10812, https://doi.org/10.1021/jp9026817.
[51] R. Klajn, Spiropyran-based dynamic materials, Chem. Soc. Rev. 43 (2014) 148–184, https://doi.org/10.1039/C3CS60181A.
[52] M.S.A. Abdel-Mottaleb, M. Saif, M.S. Attia, M.M. Abo-Aly, S.N. Mobarez, Lanthanide complexes of spiropyran photoswitch and sensor: spectroscopic investigations and computational modelling, Photochem. Photobiol. Sci. 17 (2018) 221–230, https://doi.org/10.1039/C7PP00226B.
[53] G. Pariani, M. Quintavalla, L. Colella, L. Oggioni, R. Castagna, F. Ortica, C. Bertarelli, A. Bianco, New insight into the fatigue resistance of photochromic 1,2-diarylethenes, J. Phys. Chem. C 121 (2017) 23592–23598, https://doi.org/10.1021/acs.jpcc.7b04848.